2020-01-0168 Published 14 Apr 2020

Conjugate Heat Transfer CFD Analysis of an Oil Cooled Automotive Electrical Motor

Chiranth Srinivasan Simerics, Inc.

Xiaofeng Yang and Jeff Schlautman General Motors LLC

Deming Wang Simerics, Inc.

Srihari Gangaraj General Motors LLC

Citation: Srinivasan, C., Yang, X., Schlautman, J., Wang, D. et al., "Conjugate Heat Transfer CFD Analysis of an Oil Cooled Automotive Electrical Motor," SAE Technical Paper 2020-01-0168, 2020, doi:10.4271/2020-01-0168.

Abstract

This study brings to forefront the analysis capability of CFD for the oil-cooling of an Electric-Motor (E-Motor) powering an automobile. With the rapid increase in electrically powered vehicle, there is an increasing need in the CFD modeling community to perform virtual simulations of the E-Motors to determine the viability of the designs and their performance capabilities. The thermal predictions are extremely vital as they have tremendous impact on the design, spacing and sizes of these motors. In this paper, with the Simerics, Inc. software, Simerics-MP+®, a complete three dimensional CFD with conjugate heat transfer CHT model of an Electric Motor, including all the important parts like the windings, rotor and stator laminate, endrings etc. is created. The multiphase Volume of Fluid (VOF) approach is used to model the oil flow inside this motor. Two parts of the oil flow, rotor and stator flow, both are simulated, and the net effect of the oil cooling the different solid components is predicted. The study shows the mesh capturing of complicated, intricate paths with relative ease combined with the robust high fidelity interface capturing VOF scheme with rapid turnaround times makes it a very attractive tool for design studies. Thermal results obtained from simulations are compared to physical test data obtained from thermocouple measurements and very good agreement is found.

Introduction

Thermal analysis of electrical motors has garnered as much attention as electromagnetic analysis in the recent times. The necessity to increasingly miniaturize the system, while ensuring it to be highly efficient and cost effective provides some challenges that can be better understood using simulations. The simulation environment provides fertile grounds to virtually test new topologies and new materials without drastic expenditures to ascertain the possibilities of achieving end objectives of reduced size, reduced costs and reduced weight while maintaining high efficiency requirements. Simulations can also provide insights into the temperature hotspots and thermal fatigue scenarios that can ascertain if the design is reliable and consistently performing optimally. The thermal field of an electrical motor is one of the most critical aspects that determine its net effective output [1]. It should also be pointed out here that the electromagnetic losses have a strong dependency on the temperature field and hence there is a symbiosis that makes thermal analysis even more crucial.

Three different simulation practices can be utilized to model the thermal systems in electric motors. Network model with lumped parameter type of analysis offers a realistic methodology to study the thermal aspects of an electrical motor system. The complexities handled can be quite diverse and the really fast solutions can be obtained for transient start-up analysis or transient varying load condition analysis [2,3,4,5]. The advantages such models offer are that they are extremely fast to run and can take a coupled approach incorporating the interdependencies of the electromagnet field on the temperature field and vice-versa [2,3]. However, on the downside, such models do involve some amount of empiricisms combined to the requirements of investing large amounts of time in assembling the various coefficients and details to setup these large networks.

CAE offers a significant benefit to the modeling of these types of systems as it removes a lot of empiricisms associated with the modeling. The real geometry can be modeled as is, or as to close to as it is and the predictions can be as realistic as in reality. But, the CAE software in market can be sometimes very limiting to the geometries that can be modeled. Especially, in this type of modeling, the complicated shapes of the winding, capturing the oil distribution patterns in these windings, model replicating the smalls gaps between the several different solid components all pose substantial challenges to the modeling of such systems. The two broad categories of CAE analysis are Finite Element Analysis (FEA) and Computational Fluid Dynamics (CFD).

In this paper, a method development study understanding the complexities of a particular E-Motor system and capabilities using commercial CFD/CAE software, Simerics-MP+, in modeling the combined rotor and stator flows inside an E-Motor are presented. The study shows the robustness of CAE in its ability to model the complicated nature of the physics at hand while providing a unique 3D picture of the inner workings of the system. System temperatures in different parts of the system are predicted using a Conjugate Heat Transfer (CHT) model.

Background

The history of the use of CFD for understanding the inner workings of an electrical machine can be traced back 20 years. The lack of large infrastructures in terms of computational resources as well as the rudimentary nature of CFD capabilities of those times meant that the applications of CFD for such system studies were very academic for really small scale simplistic cases. Only some fundamental understanding could be garnered from such studies and they carried hardly, if any, impact on the engineering and design aspects of such systems. Few earliest works [6,7] looked at cooling of a large air-cooled synchronous generator or motor. The commercial CFD code, Fluent was utilized for their work. It involved only a single phase, air, with a rotating component, rotor blade, inside. An assortment of assumptions involved simplifying some details of the geometry to be modeled and using the periodic boundary conditions. The studies looked at the turbulence model, varying the mesh to get mesh independent results. The Moving Reference Frame (MRF) approach was used to model the rotational motor. The predicted Heat Transfer Coefficient (HTC) on rotor windings followed the trends of experiment but the absolute predictions were at least lower by 30%. Studies of Connor et al. [8] also showed the capabilities of CFD in modeling capturing the flow rate and torque with reasonable accuracy in an air cooled synchronous generator. Recent developments in cooling studies of electrical motors have established the designs with direct oil spray cooling of the heat generating solids [9, 10, 11].

Ponomarev et al. [12] studied the oil cooling of a permanent magnet synchronous machine. It was a conjugate heat transfer model including both the fluid and the solid. Heat sources are imposed on the copper region, steel lamination region, and PM (Permanent Magnet). The RANS (Reynolds Averaged Navier Stokes) k-ε model was used to simulate the turbulent flow. The model was simplified to include only $1/18^{th}$ sector model and the rotor solids were assumed to be stationary. Given all these assumptions, they still found that the temperature distributions to be quite realistic showing higher temperatures in the center regions of the copper windings compared to the ends in the regions of about 160^0C. They discuss the ability of CFD to provide a much clearer picture of the physics at work but also point out the complexity and large times spent on developing a CFD model and running it in big powerful computers. In another study [13], the direct oil cooling of the electric motor is simulated using Fluent, Inc., to determine the effectiveness of the thermal guiding flow structures. Once again, in this case, the model was simplified in order to reduce calculation times and the solid components are not modeled. Also, only a sector is modeled, with periodic boundary conditions, to save mesh and computational time. The end-turn cooling is not modeled as the authors talk about the sophisticated nature of such a two-phase-flow problem and they use test data to provide the HTC in their simulation. Research work of Connor et al. [14] recently published also deals with CFD analysis of oil impingement on end-windings. A laboratory test rig was designed carefully and developed to test the dynamics of the oil impingement on the end-windings and then compare the behavior to that of CFD simulations. This model also involves some simplifications to the geometries while generating the CFD model, assuming symmetry and the flow was not multiphase, as in reality. Parametric study varying the geometric dimensions of the delivery pipe diameters and plenum sizes were performed to showcase the versatility of CFD. Previous work [15] has also shown the capability of CFD in influencing design decisions for cooling jackets in electrical machines. Previous work also have looked at oil cooling of windings [16].

Due to the higher power densities of these electrical machines, the direct oil cooling of the stator windings and the rotor end rings is the most preferred method for heat removal. As these CFD studies detailed show, the ability of CFD in developmental capabilities in such type of systems can be crucial to better designs for effective heat removal and improved efficiencies. In this paper, a CFD methodology development process is detailed using a proprietary software, Simerics-MP+, for an electrical motor that is cooled by spray cooling of oil on its end windings and end rings. Some of the highlights of this model development will include:

1. Conjugate Heat Transfer.
2. Rotating mesh for rotor spray modeling.
3. No geometric simplifications with high-fidelity geometric capturing using the Simerics volume mesh.
4. High resolution interface tracking with oil and air multiphase model.
5. Comprehensive all-inclusive model for an electric system without simplifying assumptions like symmetry, sector model etc.

Mathematical Model

The approach used in the current study solves conservation equations of mass, momentum, and energy of a compressible fluid using a finite volume approach. Those conservation laws can be written in integral representation as

$$\frac{\partial}{\partial t}\int_{\Omega(t)} \rho d\Omega + \int_{\sigma} \rho\left(v - v_{\sigma}\right).nd\sigma = 0 \tag{1}$$

$$\frac{\partial}{\partial t}\int_{\Omega(t)} \rho v d\Omega + \int_{\sigma} \rho\left(\left(v - v_{\sigma}\right).n\right) v d\sigma = \int_{\sigma} \tilde{\tau}.n d\sigma - \int_{\sigma} p n d\sigma + \int_{\Omega} f d\Omega \tag{2}$$

$$\frac{\partial}{\partial t}\int_{\Omega(t)} \rho E d\Omega + \int_{\sigma} \rho\left(\left(v - v_{\sigma}\right).n\right) E d\sigma = \int_{\sigma} k \nabla T.n d\sigma - \int_{\sigma} p v.n d\sigma + \int_{\sigma} \left(v.\tilde{\tau}\right).n d\sigma + \int_{\Omega} f.v d\Omega \tag{3}$$

For solution within the solid model, only the conduction part of Eq. 3 was solved. The standard $k - \varepsilon$ two-equation model with wall function is used to account for turbulence,

$$\frac{\partial}{\partial t}\int_{\Omega(t)} \rho k d\Omega + \int_{\sigma} \rho\left(\left(v - v_{\sigma}\right).n\right) k d\sigma = \int_{\sigma} \left(\mu + \frac{\mu_t}{\sigma_k}\right)\left(\nabla k.n\right) d\sigma + \int_{\Omega} \left(G_t - \rho \epsilon\right) d\Omega \tag{4}$$

$$\frac{\partial}{\partial t}\int_{\Omega(t)} \rho \varepsilon d\Omega + \int_{\sigma} \rho\left(\left(v - v_{\sigma}\right).n\right) \varepsilon d\sigma = \int_{\sigma} \left(\mu + \frac{\mu_t}{\sigma_\varepsilon}\right)\left(\nabla \varepsilon.n\right) d\sigma + \int_{\Omega} \left(C_1 G_t \frac{\varepsilon}{k} - C_2 \rho \frac{\varepsilon^2}{k}\right) d\Omega \tag{5}$$

VOF Model for Multiphase

VOF models are widely used in simulation of two phase flow [16, 17]. VOF solves a set of scalar transport equations representing the fraction of the volume each fluid component occupies in every computational cell. The transport equation of the volume fraction for each fluid component can be written as:

$$\frac{\partial}{\partial t}\int_{\Omega(t)} \rho_i F_i d\Omega + \int_{\sigma} \rho_i \left(v - v_{\sigma}\right).n F_i d\sigma = 0 \tag{6}$$

Where Fi is the volume fraction of the ith fluid component, and ρi is the local density of i^{th} fluid component. The weighted mixture density of the fluid in equation (1) to (5) are then calculated as:

$$\rho = \sum \rho_i F_i \tag{7}$$

Both implicit and explicit methods can be used to solve the equation. High Resolution Interface Capturing (HRIC) scheme can be used for the convective term in the transport equation. The VOF model within used in the current approach has also been validated extensively for multiphase flow without including the energy equation [18, 19] and for multiphase flow including the energy equation [20].

"Mixed Timescale Coupling"

For obtaining the temperature field inside the E-Motor, instead of a complete conjugate heat transfer solution, a "mixed timescale coupling" approach is used to solve for the thermal field. This approach has been previously utilized in an earlier work for piston cooling heat transfer study [20]. A short description of its implementation is provided here with further details in the referred publication. A pictorial representation of the concept is shown in Figure 1. The reason that this approach can be implemented here is the large differences in timescale for the fluid and solid thermal problems. Due to the high thermal inertia of the solid materials, the solid thermal field can take a few minutes to get to a thermal equilibrium but the fluid thermal field can stabilize within few seconds. Due to the high thermal inertia, with a few seconds, typical for the fluid simulation, the solid temperatures do not undergo significant change. The procedure utilized here is as follows:

1. At some transient time instant of the simulation, the fluid velocity, pressure and oil volume fraction fields obtained at that moment in time are used to solve the convection heat transfer.
2. For all the surfaces of fluid in contact with the solid, the heat flux in the form of Heat Transfer Coefficient (HTC) and Reference Temperature (T_{ref}) is mapped to the solid simulation.
3. The steady state solution for the solid heat transfer simulation is performed by mapping the HTC and T_{ref} on all the conjugate surfaces with the fluid. At the end of convergence, the results for the temperature fields on the solid surfaces are then mapped back to the fluid simulation.
4. The procedure is repeated with step 2 and 3 iteratively till the heat fluxes between the fluid and solid simulations balance for all the surfaces and the temperatures on all the solids undergo no further change.

FIGURE 1 Shows a pictorial representation of the "mixed timescale coupling" approach used for studying the conjugate heat transfer.

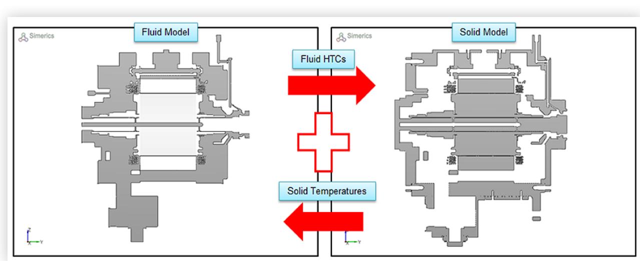

FIGURE 2 Sum of heat fluxes on all the conjugate surfaces scaled with a reference heat flux plotted from fluid side and solid side for each back and forth fluid-solid iteration.

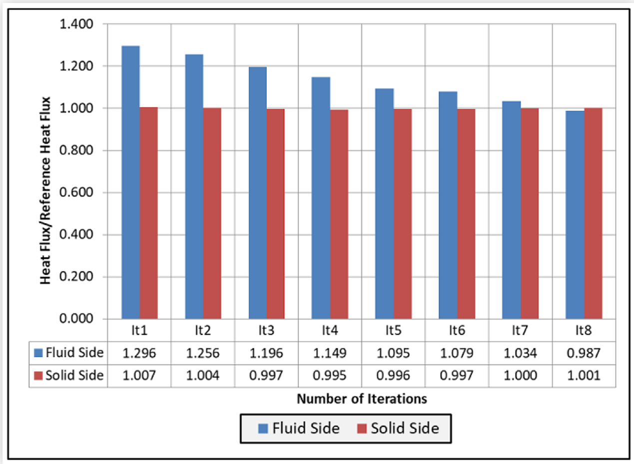

FIGURE 3 The surface averaged temperatures scaled with some reference temperature, on four different conjugate surfaces from the solid side that transfer the temperatures to the fluid side, with each fluid-solid iteration is shown.

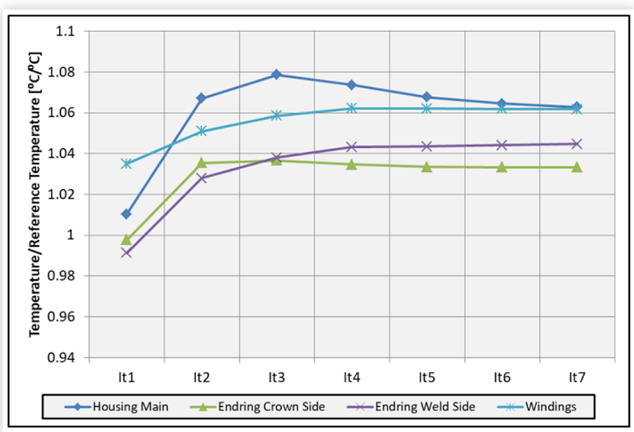

To illustrate the convergence of the heat transfer simulation, a plot is shown in Figure 2 of the heat fluxes summed up for all the conjugate surfaces between the fluid and solid model transferred from the fluid to the solid model, presented as fluid side, and from solid to fluid model, presented as solid side, for each back and forth iteration, scaled to some reference value of heat flux. Based on the initial guess in temperature on the solid surfaces, for the fluid model, the fluid heat fluxes will start at quite different values compared to the solid side heat fluxes. But, eventually after 8 fluid-solid model iterations, it is clear that the total heat fluxes balances between the fluid and solid model within less than 1.5% difference. In Figure 3, the surface averaged temperatures on four different solid surfaces scaled with a reference temperature, that transfer temperatures to the fluid model are plotted as a function of each back and forth iteration between fluid and solid model. The graph clearly shows that each of the surfaces achieve a stable operating temperature within 8 iterations between the fluid and solid simulation.

Model Details

The fluid cooling of this E-Motor is through two oil coolant pathways. The first pathway is through the rotor shaft, which we will refer to as rotor flow from hereon. The second pathway is through the cooling channels in the housing that funnels the flow into the different parts of the windings through baffles. This latter flow will be referred to as stator flow for the rest of the manuscript. Figures 6(a) and 6(a) shows a cross sectional view of the rotor and stator flow oil coolant passages.

For the rotor flow, as can be seen in Figure 6(a)(a), oil is input through an axially drilled hole in the shaft. There are four radially drilled holes through the shaft as well, a pair in two different axial locations. As the oil flows axially in through the shaft, as it encounters these four radially drilled holes, the centrifugal force of the spinning shaft solid causes the oil to start radially flowing out through these four radially drilled holes. The four radially drilled holes are placed in such a way that the oil exiting them then splashes on the end ring surfaces. Note that all these solids are rotating, as shown in Figure 6(a).

FIGURE 4 *x* cross sectional view cutting through the E-Motor showing the finer details in the geometry

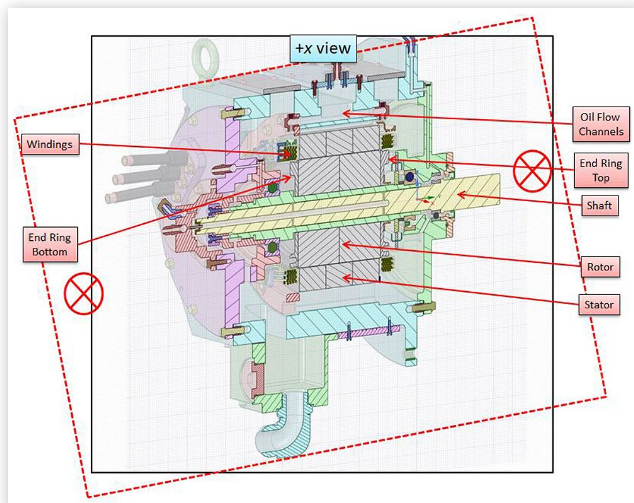

FIGURE 5 Shows an exploded view of some of the main components included in the simulation model

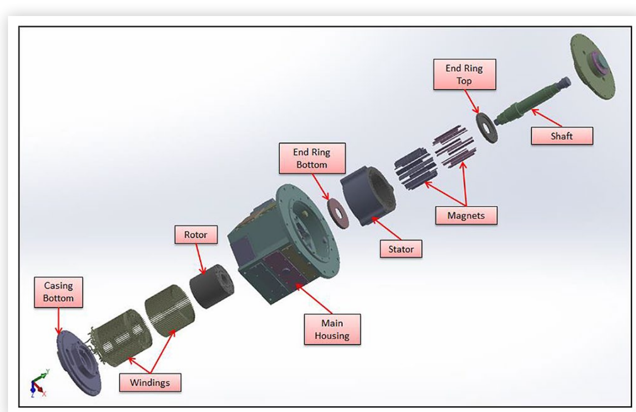

FIGURE 6(a) Shows a z-cross-sectional view of the rotor flow passages

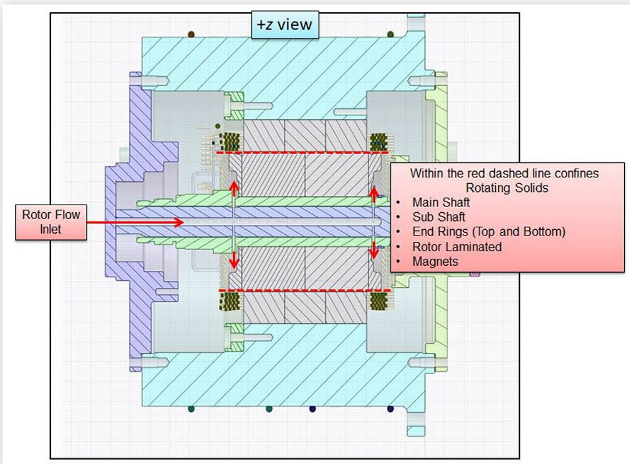

FIGURE 6(b) Shows a x-cross-sectional view of the stator flow passages

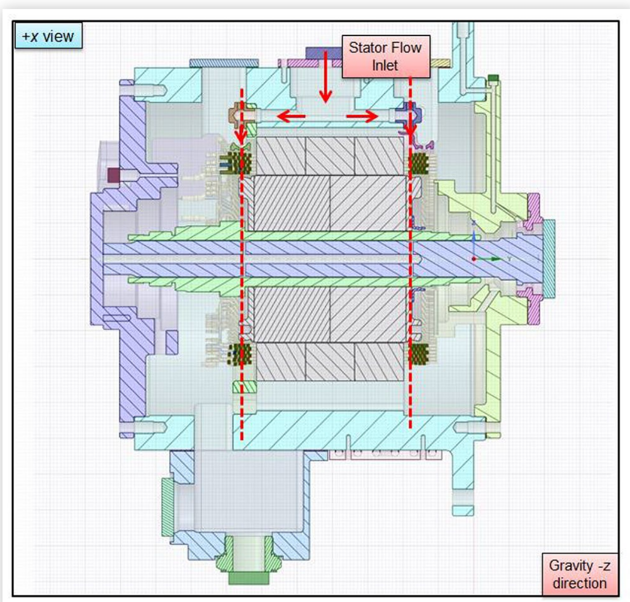

The magnets that are encased in the rotor laminate are hot and conducting heat through to the rotor laminate surface, and further down to the end rings. Hence, this heat is removed by the oil spray through the rotor flow. The relatively hot oil after it splashes on the end ring surfaces then goes further downstream to splash on the winding surfaces, removing heat from the hot winding surfaces before exiting the system.

For the stator flow, the oil flow is introduced near the center of the casing on the +z side. As the oil flows down, the gravity acting in the -z direction aids in the oil flowing down through the oil coolant passages and then there are small channels that funnel the oil through into the windings. The y directional views at the two cross-sectional planes indicated by the hashed lines in Figure 6(a)(b), the left and right lines on the crown and weld sides, respectively, are

FIGURE 7 Shows the y cross-sectional views on the crown and weld sides that clearly showcases the oil coolant path through the baffles and that channels the oil flow through to the windings.

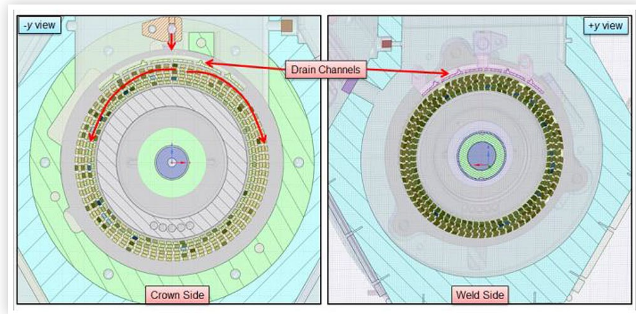

shown in Figure 7. The windings have a curvature in the circumferential direction, and combined with the fact that the channels funnel the oil at different circumferential locations of the windings, cause the oil to spread to different parts of the windings, and then flow down into the sump through the outlet port. The oil through the stator flow helps in cooling down the heated surfaces of the stator laminate, housing and mainly the windings.

From the computational stand point, the cooling problem of the E-Motor operates in two different time scales, for the rotor flow, the speed of the shaft could be substantially high. This makes the velocity high, and hence, the Courant number is large. In order to capture the oil-air interface with accuracy, the timestep for this part of the simulation needs to be really small, in order to have the Courant number around 1. For the stator flow part, due to the nature of gravity driven flow, the velocities are of relatively smaller magnitude, and hence the timestep needed to accurately resolve the oil-air interface can be larger. Another perspective of these two problems is that, in the rotor flow case, the solution is periodically repeating itself. As the results for the flow simulation, repeats itself after every revolution. The first revolution needs to be ignored, as the initial condition effects gets washed out. So, it's sufficient to run the rotor flow simulation for three revolutions, and stop it after verifying the solution doesn't change from second to third revolution. But, the stator flow simulation, the simulation needs to be run for much longer time. Since, it takes a few seconds for the oil entering the system, and the oil exiting and the system oil to balance. Depending on the dimension of the system, the input flow velocities and the design on the windings and baffles, the time duration for simulation here could be varying from 30s, all the way up to few minutes. Once, the oil in the system balances, and the inlet and outlet flow rates of oil is balanced, the simulation has reached a quasi-steady state and can be stopped. So, the challenge in this problem, as a whole, is two different time scales of operations for the rotor and stator flow, and two different time ranges the simulation needs to be performed to achieve time-independent results. But, the favorable storyline is that for the rotor flow, even though the timestep needs to be small, the relative amount of time that it needs to be run for is small as well, and similarly for the stator flow, even though it needs to be run for a longer duration in physical time, the timestep can be larger to help in running it fast enough.

Before jumping into the simulation of the entire E-Motor that includes both the rotor and stator flows some details of the simulation with the rotor and stator flow run independently is first presented.

Rotor Flow Simulation

The rotor flow model is shown in Figure 8 with the oil volume fractions represented by the color contours, magenta representing pure oil with blue representing pure air. For the rotor flow simulation, 100% oil is input through the axially drilled hole at a value of 1 unit. This is volumetric flow rate of oil scaled with an arbitrary value of flow rate, for confidentiality purposes, and hence a dimensionless number representing flow rate. The axial and radial surfaces on the crown and weld sides are prescribed an outlet atmospheric boundary condition. Ideally, to verify the filling of oil in the crown and weld side, the system needs to be completely filled with air and no oil and let the simulation run to periodic steady state results. But, due to run time concerns, the system is initialized with oil distribution as shown initially in Figure 8 and the simulation is performed. It has been verified separately, results of the same not being presented here, that the initial conditions do not have a bearing on the final periodic steady state solution. The mesh, as shown in Figure 9, is created using the general mesher of Simerics, which is an unstructured binary tree grid that is cut at the boundaries to confirm to the shape of the solids. Refinement zones are defined based on the possible locations of oil flow with the cells in those zones being much smaller than those outside those zones. Also, in order to capture the oil film on the endring surfaces, the surface cell sizes are also refined to really small sizes. A zoomed in insert image of the mesh showing the refinement zones and the boundary refinement can also be seen in Figure 9. The mesh for this simulation is around 30 million cells, with predominantly hexahedral elements. The simulation is run with 1 degree crank angle time step using 152 cores, and it takes about 3 hours of wall clock time to run one revolution. To achieve periodic steady state conditions, the simulation needs to be run for 3 revolutions.

FIGURE 8 Shows the 3D CFD model of the rotor flow simulation.

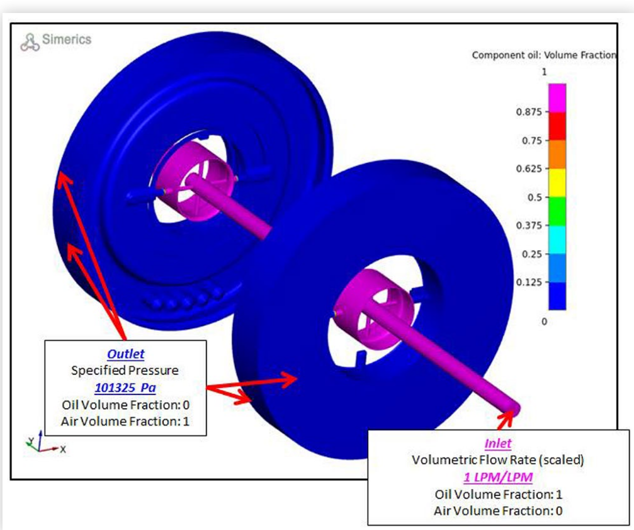

FIGURE 9 The rotor flow mesh is shown here.

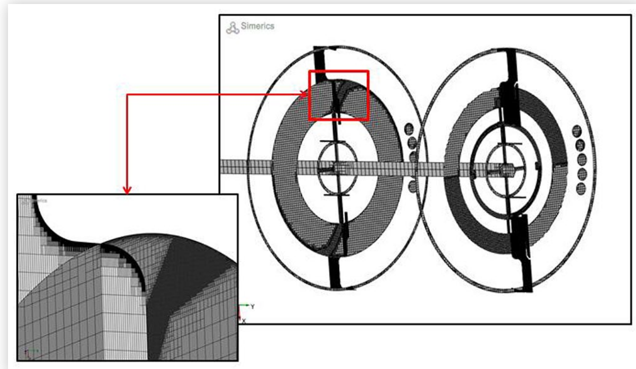

FIGURE 10 Shows the distribution of oil for the scaled value of 1 shaft speed.

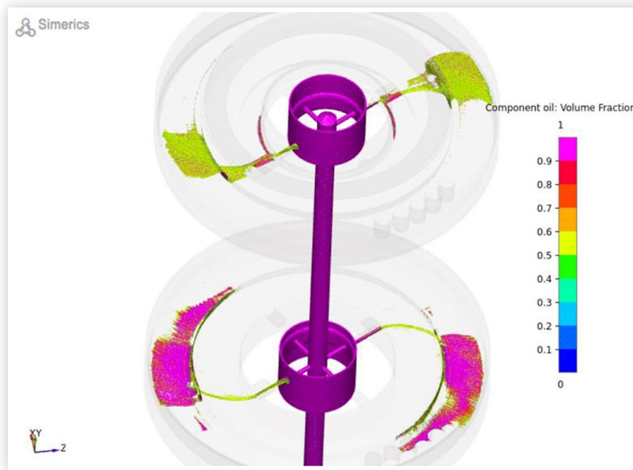

Two different speeds of the shaft are considered for this simulation; scaled values of 1 and 2.125, results for both will be presented and discussed below. The simulation result of the oil distribution exiting the radially drilled holes in the shaft and splashing on the endrings at the end of 6 revolutions for the first speed case is illustrated in Figure 10. The quantitative values of the flow rates at this shaft speed through the crown and weld sides, normalized to a reference flow rate value, as a function of time are shown in the graph in Figure 11. Two observations apparent from this plot are; (a) the flow rates stabilizes within 0.02 secs, (b) the flow of oil through the two, crown and weld, ends are nearly identical. The crown end is receiving around 0.52 while the weld side gets 0.48 of the total 1. A view of the oil splash patterns formed on the endrings as a result of the oil flow is shown in Figure 12. Quantitatively, at this shaft speed, ~11.6% and ~4.9% of the crown side and weld side endring surface areas, respectively, are covered with the oil film.

Similar results for the 2.125 shaft speed rotation case are presented below. The Figure 13 shows the graph of oil

FIGURE 11 Plot showing the sum of the oil volumetric flow rates through the two drilled holes on the crown side and the weld side for the scaled value of 1 shaft speed.

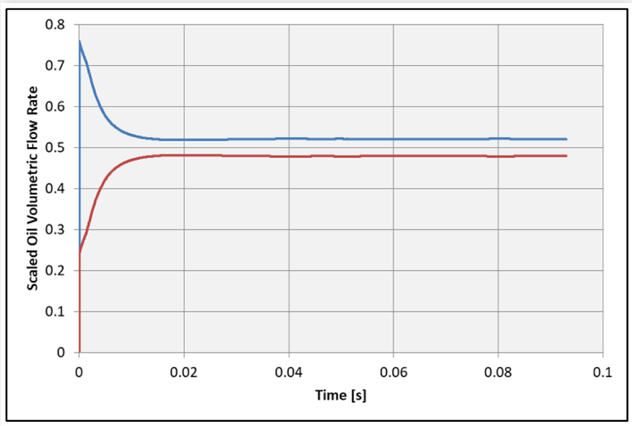

FIGURE 12 Shows the oil splash patterns on the endring surfaces, left contour represents the endring on the crown side and right contour represents the endring on the weld side, at scaled value of 1 shaft speed.

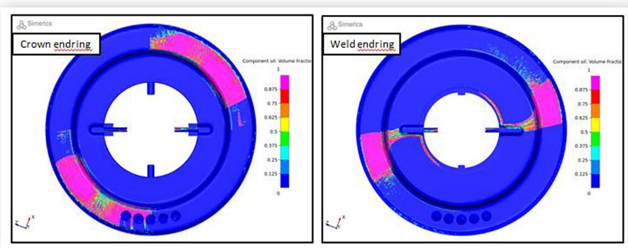

FIGURE 13 Plot showing the sum of the oil volumetric flow rates through the two drilled holes on the crown side and the weld side for the scaled value of 2.125 shaft speed.

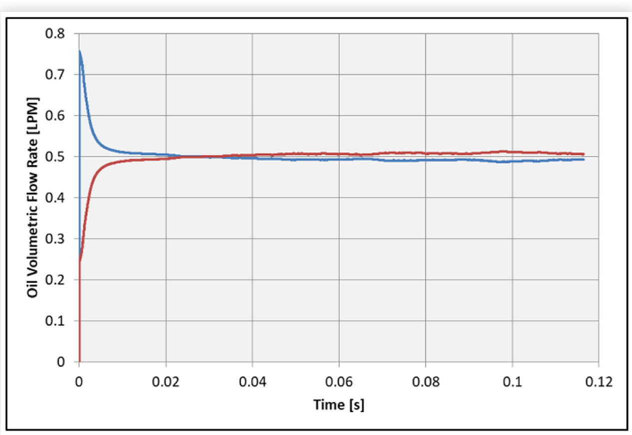

volumetric flow rates, normalized with a reference value, plotted as a function of time for the 2.125 shaft speed case with the blue and red line representing the crown and weld side flows, respectively. The volumetric flow rates of oil to the crown and weld side are nearly an equal split, with the values ~0.494 and ~0.506 to the crown and weld sides, respectively. In Figure 14, the oil splash patterns on the crown and weld side endring surfaces are shown. At this speed, ~5.8% and ~3.6% area of the crown and weld side endring surfaces, respectively, are wetted with oil. One of the important points worthy of noting here is the integrated mass balance error of oil in the system for both speeds of the simulation is within 0.1%.

FIGURE 14 Shows the oil splash patterns on the endring surfaces, left contour represents the endring on the crown side and right contour represents the endring on the weld side, at scaled value of 2.125 shaft speed.

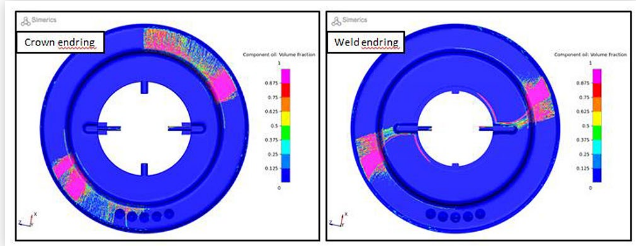

Stator Flow Simulation

The stator flow model is shown in Figure 15. 100% oil at 1 unit, a normalized value of flow rate, is input through inlet boundary on the +z side near the center of the housing. The bottom hole in the -z side is open to the sump and prescribed an outlet boundary with atmospheric pressure. The gravity direction is specified as -z direction, and the system is initialized with 100% air initially. The cross sectional view (x=0) of the stator flow mesh is shown in Figure 16. Similar to the rotor flow case, the unstructured binary tree mesh with predominantly hexahedral cells cut to the solid definition is used for the meshing. The refinement zones with finer cells are implemented in regions of expected oil flow and coarser mesh in other regions. The y cross sectional views through the two

FIGURE 15 Shows the 3D CFD model of the stator flow simulation.

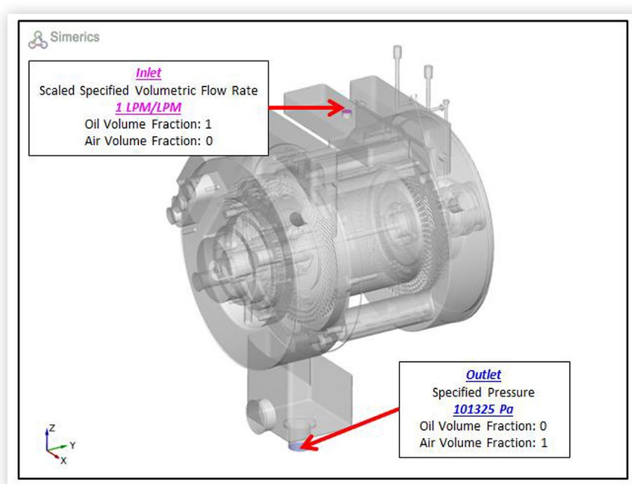

FIGURE 16 The *x*=0 sectional view of the stator flow mesh is shown here.

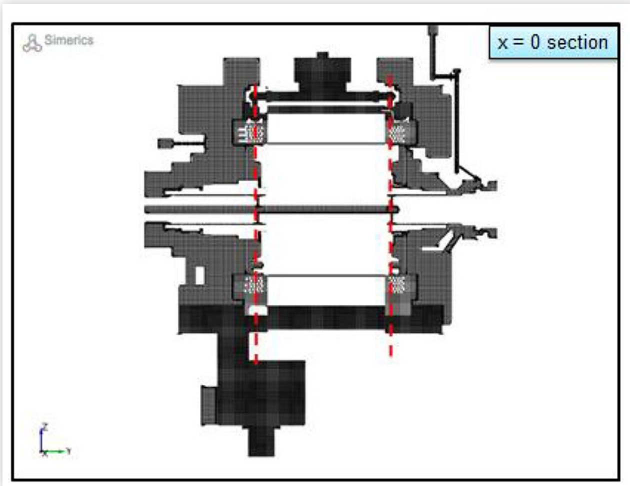

FIGURE 17 Shows the two *y* sectional view of the mesh through the crown side windings on the left, and the weld side windings on the right.

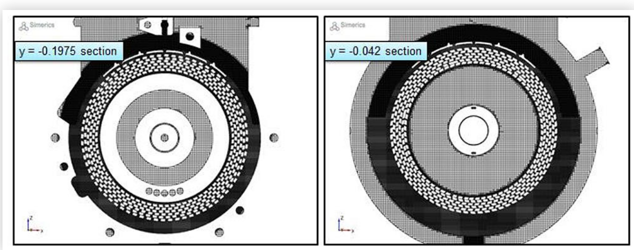

hashed lines in Figure 16 are shown in Figure 17, with the left picture representing a cut section view through the crown side windings and the right picture representing a cut section view through the weld side windings. The mesh is an automatic mesher that determines the size of the cells necessary to resolve the solid with accurate resolution. The complexity of such a model needs to be emphasized here. There are 1000s of solids parts in the model, and there is two-fold need to accurately resolve these solids with high fidelity: (a) cooling fluid flow passages captured accurately resulting in the correct oil flow distributions and (b) the heating and cooling patterns in the system will be accurately captured and the resultant solid conduction and fluid convection can be accurately computed in the simulations. In Figure 18, a side-by-side comparison of the CAD surface and resolved mesh surface is shown demonstrating the accurate resolution of the complicated solid structure of the windings. The stator flow model mesh is ~87 million cells, with predominantly hexahedral elements. The simulation is run with 1 millisecond timestep using 264 cores. Only the 1 rotor speed results are presented and discussed here. It runs about 2.5s physical time in 24 hours.

A snapshot of the oil flow distribution at 5s is shown for the stator flow simulations in Figure 19. The oil drops through the oil flow passages then wets the winding surfaces at different locations based on the holes available in the baffle for it to

FIGURE 18 Shows a side-by-side comparison between the solid CAD surface and the meshed surface captured by the Simerics mesh.

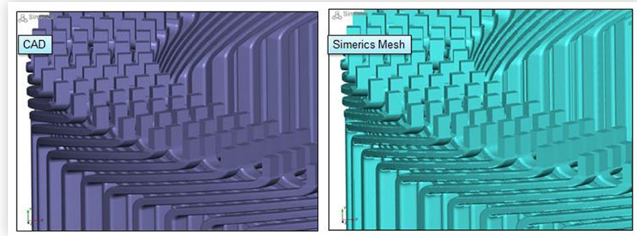

FIGURE 19 The isosurface of oil volume fraction greater than 0.5, colored by the oil volume fraction contour, at 5secs of physical time is shown here.

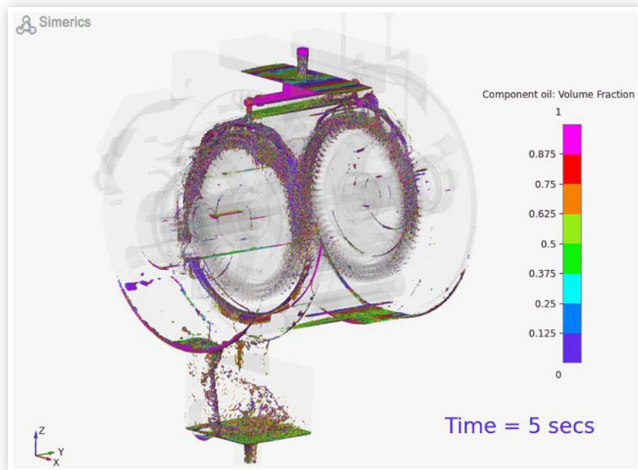

FIGURE 20 At 6s, the results for the oil volume fraction contours through x=0 and y=-0.1975 cross-sections are shown here.

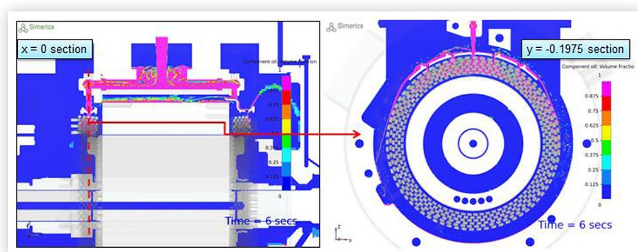

flow. It's interesting to note here that the crown side endrings does seem to get more oil compared to the weld side endrings. Figure 20 and 21 show cross sectional views of the oil volume fractions at the end of 6s of simulation. In both Figures, the x cross sectional view shows how the oil flows down and bifurcates to the crown and weld side and the y cross sectional view shows how the oil flow down the baffles to wet the winding surfaces. Eventually, the oil from both sides accumulates in the -z side of the housing and fall out through the outlet located closer to the crown side. One of the ways to monitor if the simulation has reached a quasi-steady state behavior is to monitor the oil wetted area fraction on different solid

FIGURE 21 At 6s, the results for the oil volume fraction contours through x=0 and y=-0.042 cross-sections are shown here.

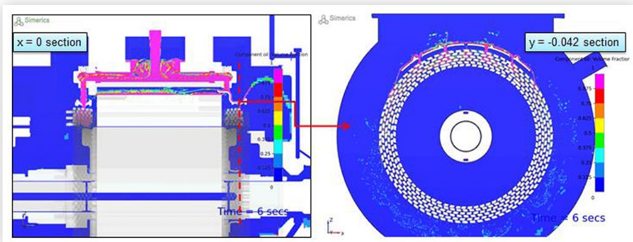

FIGURE 22 The oil wetted area fraction on the different solid surfaces plotted as a function of time is shown.

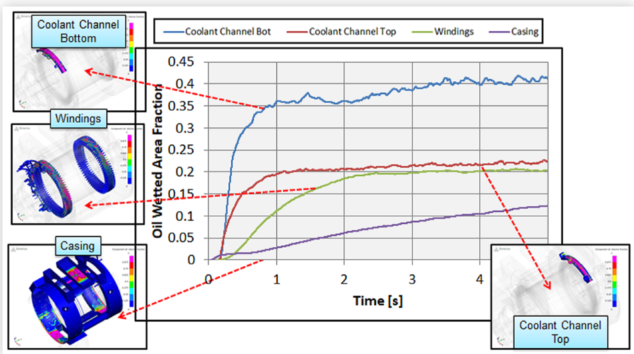

surfaces. This quantity is a measure of the fraction of area of the total area that is wetted by oil. As can be seen in Figure 22, once the solution reaches a quasi-steady state behavior, the oil wetted area fraction as a function of time remains more or less steady. Four different solid surfaces are chosen for this plot. The coolant channels on the bottom and top, meaning, crown and weld sides, reach a fraction of oil about ~0.4 and ~0.2 around ~3s. Similarly, the winding surfaces also reach a plateau of oil area fraction ~0.2 around ~3s. But, the casing surface oil wetted area fraction keeps increasing still as even after 5s the casing is still wetting with more and more oil.

Combined Model

Now, some model details with results and discussion of the combined model that includes the rotor and stator flow all in one model are presented. In Figure 23, an x and y cross sectional view of the mesh of the combined model is shown. Noticeable here is the finer mesh on the rotor flow side. The meshes for the rotor and stator flow, presented earlier in the manuscript, are combined here together to make up this combined grid, which is 117 million elements of predominantly hexahedral shape. The computational methodology developed to run this case with the rotor and stator flows both in a single model, which has the two different timesteps, is confidential and is not detailed in this paper. However, the results of the simulation are presented.

FIGURE 23 Mesh of the model with rotor and stator flow both in a single model, called the combined model, shown here.

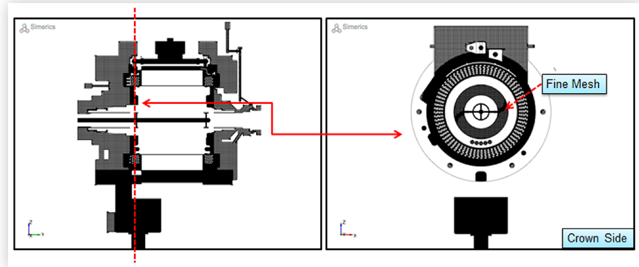

FIGURE 24 Isosurface of volume of oil greater than 0.5, after the simulation is performed for both rotor and stator flow together for ~21s.

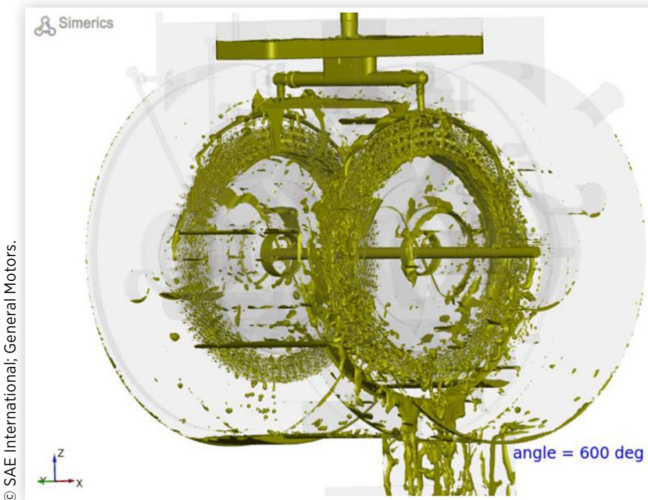

The flow rates input are the same 1 non-dimensional value, now on both the rotor and stator flow inlets. The rotational speed of the system is set at 2.125 rotor speed. The simulation is run for roughly 21s. The results for the oil volume fraction represented by an isosurface of oil greater than 0.5, is shown in Figure 21. The results show that the oil draining down from the +z side inlet, spreads through the two channels on either side, flowing down the windings wetting both the crown and weld sides and exits the system from the bottom. The rotor flow of oil exiting the radially drilled holes in the shaft and forming a film on the crown and weld side endrings can also be seen. This oil then goes further downstream to hit the windings and exit the system. In Figure 25, a plot measuring the oil volumetric flow rate through the 4 radially drilled holes in the shaft is shown as a function of time. As was seen with the rotor flow case, there is equal distribution of oil through the 4 radially drilled holes, ~0.25. Figure 26 shows the contours of oil-air distribution viewed from three different cutting planes, one at x=0, other at y=-0.1975m and the other at y=-0.042m. The results here are in corroboration with the results obtained from the cases with the rotor and stator flows run separately. Another perspective of the results are obtained from looking at it in three different sections, this

FIGURE 25 The results for the rotor flow oil volumetric flow rates through the 4 different radially drilled holes in the shaft leading to the endrings

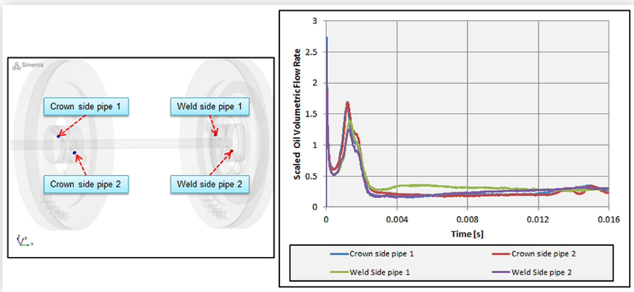

FIGURE 26 The results of oil distribution after ~21s shown from cutting planes at *x*=0, *y*=-0.1975m and *y*=-0.042m.

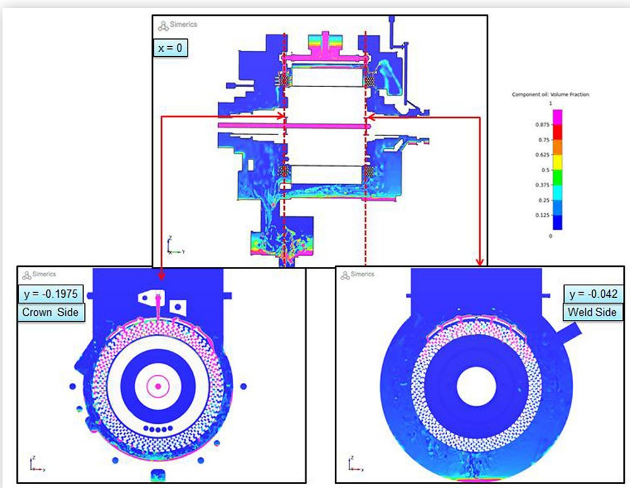

FIGURE 27 The results of oil distribution after ~21s shown from cutting planes at *z*=0, *y*=-0.1948m and *y*=-0.053m.

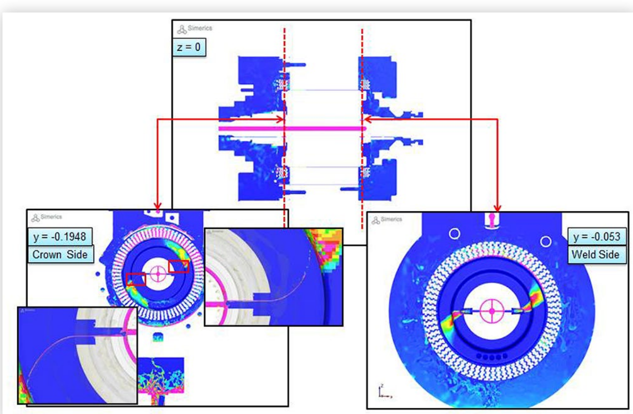

time from the z=0, y=-0.1948m and y=-0.053m in Figure 27. This sectional views also highlight the rotor flow simulation results in conjunction with the stator flow simulation results. As is apparent from the two insets, the Figure shows the jet of oil thrown out due to the centrifugal effect and hitting and splashing the endrings forming an oil film on the endring surfaces. This Figure also shows the oil spread film on the endring surfaces on top of the oil distribution through the winding surfaces.

For the combined model, it takes 120 hours (5 days) of run time to run the case till 21 secs of physical time utilizing 240 cores. The model is linearly scalable till 750 cores, potentially, and this can reduce the running time of the simulation by a factor of at least 3.

Heat Transfer Analysis

Based on the testing of this E-Motor, the heat generated in this E-Motor is measured and provided as an input to the CFD model. The values of the heat generated are distributed between the rotor, stator laminates and the windings. The Figure 28 shows the heat distributed, scaled with a reference value of heat, and the scaled values imposed as the rotor iron loss, stator iron loss and windings loss. The mesh for the solid model is 54 million cells, and it resolves all the different solid components to a finer detail. To simulate conjugate heat transfer, the "mixed timescale coupling" approach detailed in the namesake section earlier is utilized. For the heat transfer results presented and discussed below, the flow field results at ~21s is used to set the velocity, pressure and oil distribution fields in the fluid flow model. The heat transfer is solved for both the fluid and solid using steady state simulation. For the fluid simulation, the convection is solved based on the oil-air distribution and the velocity field at the particular instance of ~21s. Then the solution for the heat flux in the form of HTC and T_{ref} is loaded into the solid system and the solid simulation is run for the conduction heat transfer. This process is carried on back and forth till the solutions for the heat transport converge. Please refer to the previous description of the "mixed timescale coupling" heat transfer approach for further details. For the solid heat transfer simulation, the properties are from Table 1 shown below.

The results of the temperature distribution show that the inlet oil coming in at low temperatures help reduce the temperatures on the surfaces of the endrings and windings. The regions closer to the inlet ports see lower temperatures,

FIGURE 28 Shows the measured heat distributed between the three different solids as rotor iron loss, stator iron loss and windings loss in dimensional units of Watts normalized by Watts.

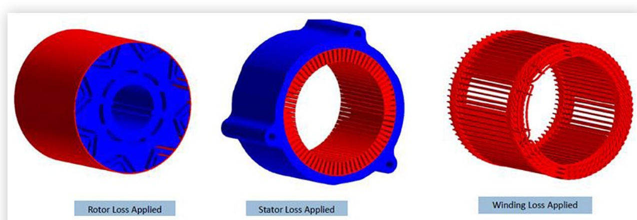

Rotor Iron Loss	Stator Iron Loss	Winding Loss
0.17	0.4	0.43

All Values are scaled with a reference heat loss value

TABLE 1 Shows for the different components, the material type along with the material property, namely, the density, specific heat and thermal conductivity.

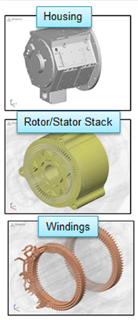

Components	Material	Density	Specific Heat	Thermal conductivity
Housings	Cast Al	2823	963	92
Stator/ Rotor stack	Laminated Steel	7870	480	35 (radial & tangential) 17(axial)
Windings	Pure Copper	8940	386	400
Coolant Channel	Plastic	1100	692	0.9
Magnets	Magnets	7500	440	9
Shaft	Steel	7830	434	64
Connection Ring	PPA-GF35 Dupont Zytel	1470	2920	0.31

while the regions farther away see higher temperatures. But, consistently oil wetted portions of the windings and endrings show lower temperatures than those not wetted by oil. The Figure 29 shows the temperature distribution in the two cutting planes at x=0 and z=0. The oil dropping down from the stator flow inlet and rotor flow inlet cools down those passages to the inlet oil temperature levels but the regions farther away from these inlets show increased temperatures in the green and yellow levels. Results of the temperature distribution in two y sectional views, one cutting through the crown end and one through the weld end is shown in Figure 30. Noticeable from the Figure 30 are blue cold traces in the regions where the cold oil is entering to take heat from the solids. And from these two views the traces where the rotor flow oil film removes heat from the solid endrings can be seen, especially in the right weld side picture. The 3D solid temperatures on the rotor, stator and windings are shown in Figure 31 as three pictures. The rotor distribution is almost symmetric about the center axis, while the stator and winding solid temperatures show lower temperatures near the stator inlet facing side compared to the outlet facing side. Also, the crown side temperatures on the windings are lower than the weld side temperatures. This is once again consistent with more oil flowing from the stator flow to the crown side than the weld side.

Finally, the normalized temperatures are compared between the experimental measurements and Simerics simulation using 24 different thermocouple locations, 12 on the crown side and 12 on the weld side of the windings. It's clear from the comparisons that the simulation captures the exact temperature distribution patterns to that in the experimental testing. The smaller values of temperatures in CFD on probes 4 to 9 and probes 17-21 are similar to that seen in the test data. The comparisons of the absolute values also show temperature

FIGURE 29 Shows the scaled temperature distribution in the x=0 and z=0 cross-sectional planes. The temperatures scaled with a reference temperature are plotted here.

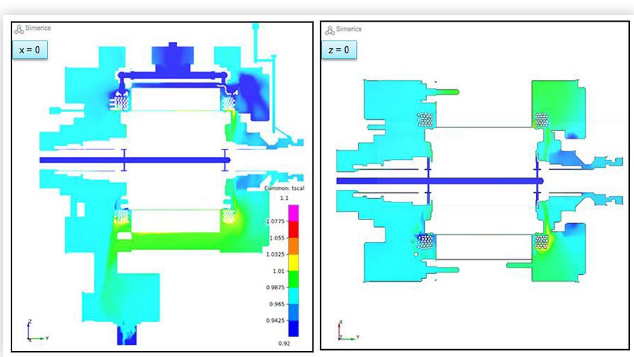

FIGURE 30 Shows the scaled temperature distribution in two y-cross sectional planes on the crown side and weld side of the E-Motor.

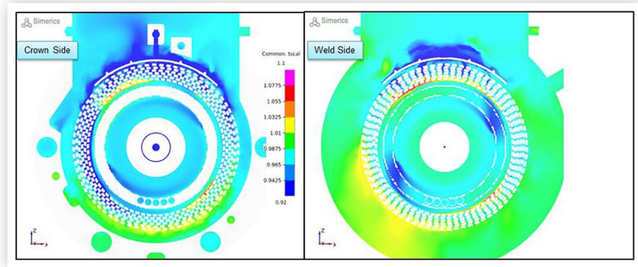

FIGURE 31 Shows the scaled temperature distributions on the rotor laminate, stator laminate and the windings solids in the three pictures

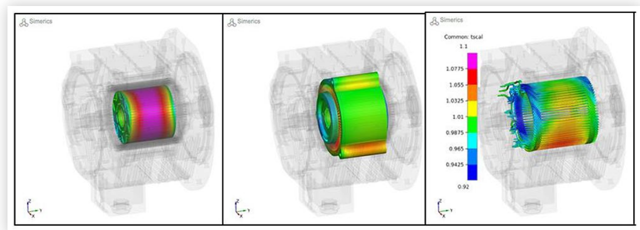

FIGURE 32 Plot shows the normalized temperatures compared between test and Simerics data in 24 different thermocouple locations in the windings.

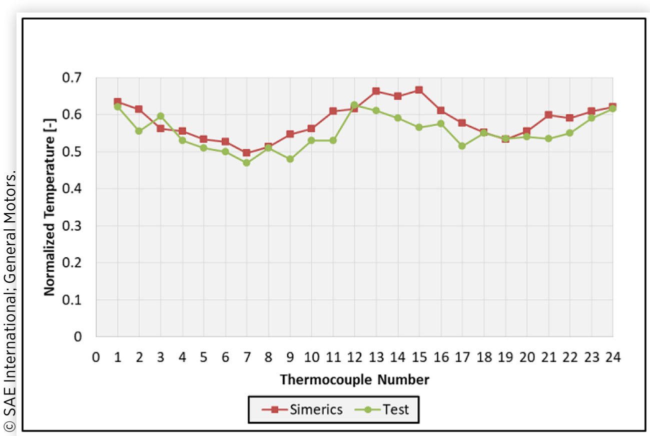

differences that are smaller than 10^0C for 75% of the probes while with an exception of one probe, the remaining 25% of the probes are still within 15^0C. The RMS (Root Mean Square) of the difference between test and Simerics data is approximately 8.85^0C.

Summary/Conclusions

The efficiencies of the electrical machines are strongly dependent on the effective heat removal. It has become highly desirable to remove heat directly at the source, at the stator windings or rotor endrings by having cooling channels that spray oil directly on these surfaces. Accurate CFD analysis to provide design directions or provide failure analysis for such motors is a monumental task due to the strong link between the geometry, multiphase fluid flow, heat loss and electrical losses. The geometries are extremely complicated in nature, and the mesh sizes and run times can be quite significant.

In this present work, a CFD method has been developed to tackle this complicated problem in an E-Motor. A fully transient three dimensional multiphase VOF simulation with Conjugate Heat Transfer is performed using Simerics-MP+, proprietary CFD software, to predict the temperatures inside a direct oil cooled E-Motor. The results of the oil distribution patterns resulting from both rotor and stator flows are presented in detail. The heat loads are currently a source input into the simulation, but internal developments have already been successful in coupling an electro-magnetic solver, JMAG, with Simerics-MP+ in making the solution even more robust and completely predictive. Temperatures results are compared to test measurements and good correlations are observed between the two.

Even with capturing all the complicated details of the geometry, the setup and run times are in the order of 5 days, with 240 dedicated cores to run the simulation. With the sophisticated nature of results that the study can produce, it offers a glimpse into the future of CFD as a tool that can lead to much faster design modifications compared to physical testing in such electrical machines.

References

1. Staton, D.A. and Cavagnino, A., "Convection Heat Transfer and Flow Calculations Suitable for Electric Machines Thermal Models," *IEEE Transactions on Industrial Electronics* 55(10):3509-3516, Oct. 2008.
2. Mezani, S., Talorabet, N., and Laporte, B., "A Combined Electromagnetic and Thermal Analysis of Induction Motors," *IEEE Trans. Magn.* 41(5):1572-1575, May 2005.
3. Dorrrell, D.G., Staton, D.A., Hahout, J., Hawkins, D., and McGilp, M.I., "Linked Electromagnetic and Thermal Modelling of a Permanent Magnet Motor," in *Proc. IEEE PEMD*, Dublin, Ireland, Apr. 2006, 536-540.
4. Mellor, P., Roberts, D., and Turner, D., "Lumped Parameter Thermal Model for Electrical Machines of TEFC Design," *Proc. Inst. Elect. Eng.* 138(5):205-218, Sep. 1991.
5. Boglietti, A., Cavagnino, A., Lazzari, M., and Pastorelli, M., "A Simplified Thermal Model for Variable-Speed Self-Cooled Industrial Induction Motor," *IEEE Trans. Ind. Appl.* 39(4):945-952, Jul./Aug. 2003.
6. Shanel, M., Pickering, S.J., and Lampard, D., "Application of Computational Fluid Dynamics to the Cooling of Salient Pole Electrical Machines," in *Proc. ICEM*, Espoo, Finland, Aug. 2000, Vol. 1, 338-342.
7. Pickering, S.J., Lampard, D., and Shanel, M., "Modelling Ventilation and Cooling of the Rotors of Salient Pole Machines," in *Proc. IEEE-IEMDC*, Cambridge, MA, Jun. 2001, 806-808.
8. Connor, P.H., Pickering, S.J., Gerada, C., Eastwick, C.N. et al., "Computational Fluid Dynamics Modelling of an Entire Synchronous Generator for Improved Thermal Management," *IET Electric Power Applications* 7(3):231-236, 2013.
9. Bennion, K., Rogers, S.A., and Narumanchi, S., "Electric Motor Thermal Management," Annual Progress Report for the Advanced Power Electronics and Electric Motors Program, Dec. 2013, 213-238.
10. Polikarpova, M., "Liquid Cooling Solutions for Rotating Permanent Magnet Synchronous Machines," Lappeenranta University of Technology, Finland, 2014.
11. Popescu, M., Staton, D., Boglietti, A., Cavagnino, A., Hawkins, D., and Goss, J., "Modern Heat Extraction Systems for Electrical Machines - A Review," in *2015 IEEE Workshop on Electrical Machines Design, Control and Diagnosis (WEMDCD)*, Torino, 2015, 289-296.
12. Ponomarev, P., Polikarpova, M., and Pyrhönen, J., "Thermal Modeling of Directly-Oil-Cooled Permanent Magnet Synchronous Machine," in *2012 XXth International Conference on Electrical Machines*, Marseille, 2012, 1882-1887.
13. Liu, Z., Winter, T., and Schier, M., "Direct Coil Cooling of a High Performance Switched Reluctance Machine (SRM) for EV/HEV Applications," *SAE Int. J. Alt. Power* 4(1), 2015, https://doi.org/10.4271/2015-01-1209.
14. Connor, P.H., La Rocca, A., Xu, Z., Eastwick, C.N. et al., "Numerical Investigations of Convective Phenomena of Oil Impingement on End-Windings," *The Journal of Engineering* 2019(17):4022-4026, 2019.
15. Yang, X., Fatemi, A., Nehl, T., Hao, L., Zeng, W., and Parrish, S., "Comparative Study of Three Stator Cooling Jackets for Electric Machine of Mild Hybrid Vehicle," in *2019 IEEE International Electric Machines & Drives Conference (IEMDC)*, San Diego, CA, 2019, 1202-1209.
16. Mavuru, C.M., Gangaraj, S., Dhade, R., and Dongaonkar, S., "Oil Cooled Motor 3D Thermal Analysis Simulation Approach," in *FISITA World Automotive Congress*, Chennai, India, 2018, F2018/F2018-EHV-008.
17. Ding, H., Jiang, Y., Wu, H., and Wang, J., "Two Phase Flow Simulation of Water Ring Vacuum Pump Using VOF Model," in *ASME/JSME/KSME 2015 Joint Fluids Engineering Conference*, 2015, V001T33A019-V001T33A019, American Society of Mechanical Engineers.

18. Kucinschi, B.R. and Shieh, T.-H., "Estimation of Oil Supply Time during Engine Start-Up at Very Low Temperatures," *SAE Int. J. Fuels Lubricants* 9(2):363-369, 2016.
19. Ding, H. and Jiang, Y., "CFD Simulation of an Oil Flooded Scroll Compressor Using VOF Approach," 2016.
20. Dhar, S., Godavarthi, R., Mishra, A., Bedekar, S., and Ranganathan, R., "A Transient, 3-Dimensional Multiphase CFD/Heat Transfer and Experimental Study of Oil Jet Cooled Engine Pistons," SAE Technical Paper 2019-01-0154, 2019, https://doi.org/10.4271/2019-01-0154.

Contact Information

Chiranth Srinivasan
Simerics, Inc.
39500 Orchard Hill Place,
Suite 190
Novi, Michigan 48375
(248) 513 3200 ext. 263

Deming Wang
Simerics, Inc.
39500 Orchard Hill Place,
Suite 190
Novi, Michigan 48375
(248) 513 3200 ext. 259

Definitions/Abbreviations

CFD - Computational Fluid Dynamics

CHT - Conjugate Heat Transfer

VOF - Volume of Fluid

HTC - Heat Transfer Coefficient

CAD - Computer Aided Design

T_{ref} - Reference Temperature

RMS - Root Mean Square

MRF - Multiple Reference Frame

ISSN 0148-7191